Vertically aligned montmorillonite aerogel–encapsulated polyethylene glycol with directional heat transfer paths for efficient solar thermal energy harvesting and storage

Qijing Guo, Cong Guo, Hao Yi, Feifei Jia, and Shaoxian Song

Cite this article as:

Qijing Guo, Cong Guo, Hao Yi, Feifei Jia, and Shaoxian Song, Vertically aligned montmorillonite aerogel–encapsulated polyethylene glycol with directional heat transfer paths for efficient solar thermal energy harvesting and storage, *Int. J. Miner. Metall. Mater.*, 31(2024), No. 5, pp. 907-916. https://doi.org/10.1007/s12613-023-2794-3

View the article online at SpringerLink or IJMMM Webpage.

Articles you may be interested in

Yang Hu, Chun-bao Sun, and Jue Kou, Exfoliation of poly(ethylene glycol)-intercalated graphite oxide composite in water without sonication, *Int. J. Miner. Metall. Mater.*, 27(2020), No. 6, pp. 840-845. https://doi.org/10.1007/s12613-019-1932-4

Bengisu Yilmaz, Behiye Yüksel, Gökhan Orhan, Devrim Aydin, and Zafer Utlu, Synthesis and characterization of salt-impregnated anodic aluminum oxide composites for low-grade heat storage, *Int. J. Miner. Metall. Mater.*, 27(2020), No. 1, pp. 112-118. https://doi.org/10.1007/s12613-019-1890-x

Xiao-guang Liu, Qiu-shuo Mao, Yue Jiang, Yan Li, Jia-lin Sun, and Fei-xue Huang, Preparation of Al_2O_3–SiO_2 composite aerogels and their Cu^{2+} absorption properties, *Int. J. Miner. Metall. Mater.*, 28(2021), No. 2, pp. 317-324. https://doi.org/10.1007/s12613-020-2111-3

Qiao-bao Zhang, Yong-chang Liu, and Xiao-bo Ji, Editorial for special issue on advanced materials for energy storage and conversion, *Int. J. Miner. Metall. Mater.*, 28(2021), No. 10, pp. 1545-1548. https://doi.org/10.1007/s12613-021-2354-7

Eltefat Ahmadi, Ahmad Fauzi, Hashim Hussin, Norlia Baharun, Kamar Shah Ariffin, and Sheikh Abdul Rezan, Synthesis of titanium oxycarbonitride by carbothermal reduction and nitridation of ilmenite with recycling of polyethylene terephthalate (PET), *Int. J. Miner. Metall. Mater.*, 24(2017), No. 4, pp. 444-454. https://doi.org/10.1007/s12613-017-1425-2

Qiu-wei Xing, Jiang Ma, and Yong Zhang, Phase thermal stability and mechanical properties analyses of (Cr,Fe,V)–(Ta,W) multiple-based elemental system using a compositional gradient film, *Int. J. Miner. Metall. Mater.*, 27(2020), No. 10, pp. 1379-1387. https://doi.org/10.1007/s12613-020-2063-7

IJMMM WeChat   QQ author group

Vertically aligned montmorillonite aerogel–encapsulated polyethylene glycol with directional heat transfer paths for efficient solar thermal energy harvesting and storage

Qijing Guo[1,2], *Cong Guo*[1,2], *Hao Yi*[1,2,3],✉, *Feifei Jia*[1,2,3], *and Shaoxian Song*[1,2],✉

1) Key Laboratory of Green Utilization of Critical Non-metallic Mineral Resources, Ministry of Education, Wuhan University of Technology, Wuhan 430070, China

2) School of Resources and Environmental Engineering, Wuhan University of Technology, Wuhan 430070, China

3) Hubei Key Laboratory of Mineral Resources Processing and Environment, Wuhan University of Technology, Wuhan 430070, China

Abstract: The conversion and storage of photothermal energy using phase change materials (PCMs) represent an optimal approach for harnessing clean and sustainable solar energy. Herein, we encapsulated polyethylene glycol (PEG) in montmorillonite aerogels (3D-Mt) through vacuum impregnation to prepare 3D-Mt/PEG composite PCMs. When used as a support matrix, 3D-Mt can effectively prevent PEG leakage and act as a flame-retardant barrier to reduce the flammability of PEG. Simultaneously, 3D-Mt/PEG demonstrates outstanding shape retention, increased thermal energy storage density, and commendable thermal and chemical stability. The phase transition enthalpy of 3D-Mt/PEG can reach 167.53 J/g and remains stable even after 50 heating–cooling cycles. Furthermore, the vertical sheet-like structure of 3D-Mt establishes directional heat transport channels, facilitating efficient phonon transfer. This configuration results in highly anisotropic thermal conductivities that ensure swift thermal responses and efficient heat conduction. This study addresses the shortcomings of PCMs, including the issues of leakage and inadequate flame retardancy. It achieves the development and design of 3D-Mt/PEG with ultrahigh strength, superior flame retardancy, and directional heat transfer. Therefore, this work offers a design strategy for the preparation of high-performance composite PCMs. The 3D-Mt/PEG with vertically aligned and well-ordered array structure developed in this research shows great potential for thermal management and photothermal conversion applications.

Keywords: montmorillonite aerogel; polyethylene glycol; phase change materials; solar thermal energy storage; flame retardant

1. Introduction

The utilization of clean and renewable solar energy through photothermal conversion and thermal energy storage technologies has become imperative to alleviate the energy crisis with the exacerbation of environmental pollution and energy scarcity. Phase change materials (PCMs), which can store and release latent heat during their melting and solidification, hold promise for solar energy harvesting and storage [1]. Therefore, thermal energy storage through PCMs can solve the natural disadvantages of spatiotemporal discrepancy and instability between solar thermal energy supply and demand. PCMs, as an environmentally conscious solution for solar thermal energy storage, have been applied in various domains, including solar thermal energy storage [2–4], solar desalination [5–6], building heat/cooling [7–8], smart textiles [9–11], thermal buffers for electronics [12–13], waste heat recovery [14–15], and other fields [16]. However, PCMs suffer from several major drawbacks, such as leakage, poor thermal performance, and poor flame retardancy. hindering the large-scale application in low-carbon industrial development.

The preparation of composite PCMs is an effective method for addressing the weaknesses of PCMs. Utilizing natural minerals with porous structures for PCM encapsulation is a widely adopted method that has led to the creation of numerous mineral-based composite PCMs [17–19]. For example, Qian *et al*. [20] encapsulated three types of PCMs (low-, medium-, and high-temperature PCMs) in porous diatomite through vacuum impregnation or simply mixed sintering and obtained encapsulation rates of approximately 60%. Some layered structural minerals, such as montmorillonite (Mt), kaolinite, and vermiculite, are also used to prepare composite PCMs through intercalation methods [21–22]. To illustrate, Li *et al*. [23] developed a paraffin/bentonite composite PCMs through solution intercalation. The developed PCMs achieved a latent heat capacity of 39.84 J/g and a maximum paraffin adsorption rate of 44.4%. Although the encapsulation of PCMs with mineral materials effectively alleviates the melt leakage, the thermal storage capacity of composite PCMs remains restricted due to the limited pore volume for loading pure PCMs. Microencapsulation

Springer

technology has been proven to be an effective strategy for preventing PCM melt leakage [24–26]. Sun *et al.* [27] prepared a layered PCM microcapsule functionalized with polyaniline/carbon nanotubes. This PCM had high latent heat capacity and good thermal regulation effect. Zhang *et al.* [28] prepared PCM microcapsules with melamine–formaldehyde resin as a shell through Pickering emulsion polymerization. The core material content of the microcapsules reached as high as 87%. However, microencapsulation has the disadvantages of requiring cumbersome preparation steps, complicated preparation technology, and high cost. Moreover, some microencapsulation methods need to use large amounts of toxic reagents in preparation, hindering their practical application.

Recently, three-dimensional (3D) porous aerogels have emerged as prime contenders for effectively encapsulating PCMs and improving thermal energy storage performance owing to their ultralight weight, remarkably high porosity, extensive specific surface area, and adaptable heat transfer capabilities [29–31]. Sun *et al.* [10] developed composite PCMs based on graphene aerogels by integrating paraffin into the support matrix. The developed PCMs demonstrated enhanced flexibility and excellent solar thermal conversion ability. Hong *et al.* [32] employed superwetting polypropylene aerogel as a support material to develop shape-stable composite PCMs with improved loading capacity for organic matter and thermal conductivity. Cheng *et al.* [33] combined polyethylene glycol (PEG) with cellulose nanocrystalline aerogels to fabricate phase change aerogel composites with drastically improved thermal conductivity. The mechanical strength of aerogels could affect the durability and cycling performances of composite PCMs. In our previous work, we developed several Mt aerogel-based composite PCMs with superior thermal properties, and found that Mt is effective in enhancing the mechanical strength of aerogel and composite PCMs [5,31,34].

However, Mt aerogels usually have a messy 3D network structure, resulting in long-range phonon paths and transmission paths and high thermal resistance. In contrast to aerogels with randomly interconnected pores, those with vertically aligned and well-ordered array structures contribute to efficient phonon transfer, resulting in highly anisotropic thermal conductivities and fast directional heat transfer. Furthermore, uniform transfer heat paths help address localized overheating and promote photothermal conversion efficiency. Liu *et al.* [35] demonstrated that vertically oriented composite PCMs, which boasted greater thermal conductivity than their randomly oriented counterparts, facilitated enhanced overall heat transfer, enabling swift heat flux transfer and ensuring uniform temperature distribution. Therefore, Mt aerogels with vertically aligned and well-ordered porous structures for encapsulating PCMs will provide directional heat conductive pathways and superior uniform heat transfer. Mt is a filler that is commonly used to enhance flame retardancy. Aerogels constructed with Mt will show enhanced flame retardancy while retaining high mechanical strength. 3D-Mt, a Mt aerogel with a three-dimensional vertically aligned structure, was designed to encapsulate PEG for the preparation of the 3D-Mt/PEG composite PCMs. The obtained composite PCMs are expected to show fast directional heat transfer ability and uniform thermal conduction. In addition, the composite PCMs constructed with Mt present excellent flame retardancy and strong mechanical strength. The 3D-Mt/PEG material developed in this work, which exhibits high strength, flame retardancy, and directional heat transfer capabilities, shows great potential for applications in thermal management and photothermal conversion.

2. Experimental

2.1. Materials

Sinopharm Chemical Reagent Co., Ltd. provided analytical grade chemicals, including sodium alginate, PEG, calcium chloride ($CaCl_2$), and absolute ethanol (C_2H_6O, 99.7%), which were used without further purification. Mt was sourced from Chifeng, Inner Mongolia. Deionized water with a resistivity of 18.2 MΩ·cm was generated by using a Millipore Milli-Q Direct 8/16 water purification system.

2.2. Preparation of the 3D-Mt/PEG composite PCMs

The preparation schematic of the 3D-Mt/PEG composite PCMs is depicted in Fig. 1.

(1) Preparation of 3D-Mt.

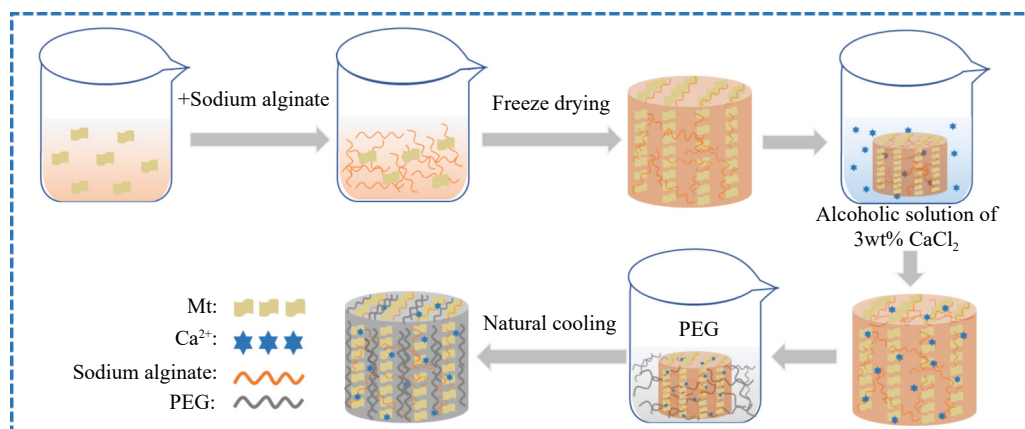First, Mt, sodium alginate, and deionized water were

Fig. 1.   Preparation schematic of the 3D-Mt/PEG composite PCMs.

mixed at a mass ratio of 1:1:20 and frozen in a refrigerator. Second, the frozen mixture was placed in a freeze-dryer for 48 h. Subsequently, lyophilized samples were immersed in an ethanolic solution of 3wt% $CaCl_2$ for 6 h. Finally, the samples were dried in an oven overnight to obtain 3D-Mt. In this work, sodium alginate and Mt were used as the basic materials for aerogel fabrication. Ca^{2+} in $CaCl_2$ can undergo ion exchange with Na^+ in sodium alginate. This reaction promotes the formation of the cross-linked network structure of sodium alginate. Given that the uncrosslinked sodium alginate is soluble in water but insoluble in ethanol, cross-linking was conducted in an ethanolic solution of $CaCl_2$.

(2) Preparation of the 3D-Mt/PEG composite PCMs.

The 3D-Mt/PEG composite PCMs were fabricated through vacuum impregnation. First, PEG was placed in a beaker and heated in an 80°C water bath until completely melted. Subsequently, the fully melted PEG was transferred to a vacuum drying oven, and the prepared 3D-Mt was immersed in the PEG melt for 4 h. The PEG melt completely filled the pores of the aerogel through vacuum impregnation. Finally, the sample was allowed to solidify at room temperature, and any excess PEG on its surface was removed.

2.3. Characterization

Samples were visually characterized through scanning electron microscopy (SEM, Phenom ProX) to analyze their morphology and structure. Fourier transform infrared (FT-IR, Nicolet 6700) spectroscopy was employed over the wavenumber range of 4000–400 cm^{-1} to examine the chemical composition of the samples. X-ray diffraction (XRD) spectra were obtained by utilizing a D8 Advance system with Cu K$_\alpha$ radiation ($\lambda = 0.15406$ nm) and scanning over the 2θ range of 5°–70°. For thermal stability assessment, thermogravimetry (TG, NETZSCH STA 449 F5) was conducted in a nitrogen atmosphere. Mass changes were tracked at a rate of 5°C/min from 20 to 600°C. Differential scanning calorimetry (DSC, Discovery DSC25, TA Instruments) was conducted at a heating/cooling rate of 2°C/min in a nitrogen atmosphere from 30 to 80°C to measure phase transition temperature and enthalpy. An infrared (IR) camera (FOTRIC 224s) was employed to record temperature distribution in the sample.

3. Results and discussion

3.1. Morphology of 3D-Mt and 3D-Mt/PEG composite PCMs

The 3D-Mt/PEG composite PCMs were prepared through vacuum impregnation. First, sodium alginate and Mt were applied to construct a 3D porous structure through self-assembly and freeze-drying (Fig. 2(a) and (b)). Fig. 2(c) provides the interconnected vertical sheet-like structure of 3D-Mt, which features numerous microscale pores that facilitate the impregnation of molten PEG. 3D-Mt was then impregnated with molten PEG through vacuum infiltration to prepare composite PCMs, as shown in Fig. 2(d) and (e). The SEM image of the 3D-Mt/PEG composite PCMs (Fig. 2(f)) illustrates that PEG has completely filled the pores of 3D-Mt. The 3D porous network effectively retains the maximum amount of PCM and prevents leakage during phase transition through robust capillary action and diffusion. In addition, the interconnected network structure can provide a conductive pathway for enhancing heat transfer in the PCM matrix.
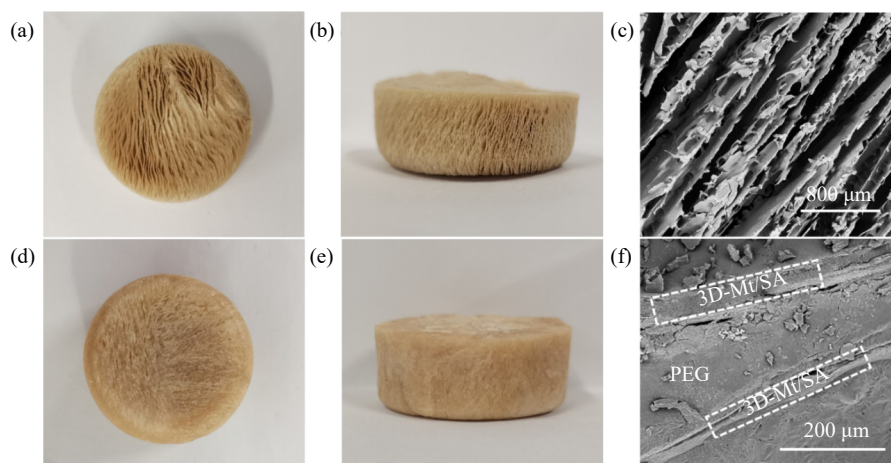

Fig. 2.   **(a) Top view, (b) side view, and (c) SEM image of 3D-Mt; (d) top view, (e) side view, and (f) SEM image of 3D-Mt/PEG composite PCMs.**

3.2. Synthesis mechanism of 3D-Mt and 3D-Mt/PEG composite PCMs

Samples were subjected to FT-IR to assess their functional groups and chemical bonds. The acquired FT-IR spectra are depicted in Fig. 3(a). The 3D-Mt samples displayed characteristic peaks corresponding to Mt and sodium alginate. Specifically, the peak observed at 3416 cm^{-1} corresponded to the stretching vibration of –OH present in Mt and sodium alginate [36–38]. The absorption peaks observed at 1627 and 1435 cm^{-1} were attributed to the stretching vibration of –COO– in sodium alginate [39–41]. Additionally, the peaks observed at 1035, 519, and 465 cm^{-1} were associated with the stretching vibration of Si–O, the bending vibration of Si–O–Al, and Si–O–Si in Mt, respectively [34,42–43].
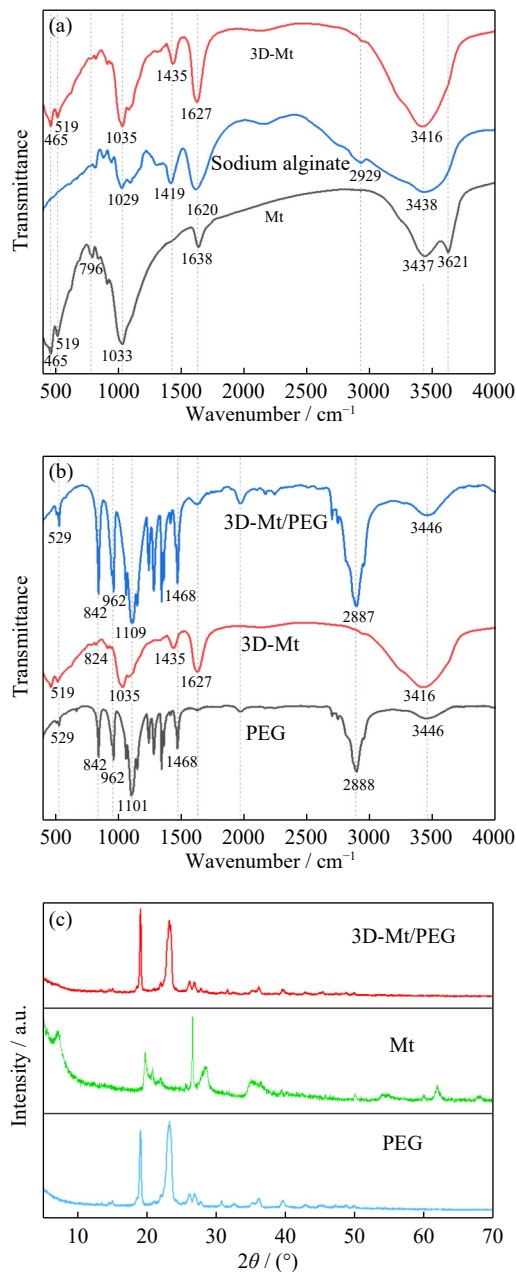
Fig. 3.   (a) FT-IR spectra of 3D-Mt, sodium alginate, and Mt, (b) FT-IR spectra of 3D-Mt/PEG composite PCMs, 3D-Mt, and PEG, and (c) XRD patterns of 3D-Mt/PEG composite PCMs, Mt, and PEG.

FT-IR was conducted to further ascertain the chemical compatibility between PEG and 3D-Mt, and the corresponding results are depicted in Fig. 3(b). As can be seen, all distinctive peaks in the 3D-Mt/PEG composite PCMs corresponded to PEG and 3D-Mt. The peak observed at 3446 cm^{-1} corresponded to the typical –OH stretching vibration presented in 3D-Mt and PEG. The peaks at 2887, 1468, 962, and 842 cm^{-1} were associated with the C–H vibration in PEG. The peak at 1109 cm^{-1} indicated the stretching vibration of C–O–C in PEG [33,44–46]. Thus, these results reveal that only physical interaction transpired between the aerogel and PEG and that no chemical reaction occurred.

Furthermore, XRD was conducted to explore the crystallization characteristics of the 3D-Mt/PEG composite PCMs

and their constituent components. Fig. 3(c) shows that the characteristic peaks of the 3D-Mt/PEG composite PCMs had not significantly changed compared with those of PEG. Typical characteristic peaks at $2\theta = 19.1°$ and 23.3° that corresponded to the (120) and (130) crystal planes of PEG, respectively, were observed. This finding indicates that PEG had successfully filled the pores of 3D-Mt. Furthermore, PEG maintained its crystalline state even after incorporation into the 3D-Mt aerogel, reflecting the excellent chemical compatibility between the PCMs and supporting matrix. FT-IR and XRD illustrate excellent chemical compatibility and robust physical interaction in the 3D-Mt/PEG composite PCMs.

3.3. Latent heat of composite PCMs

In thermal management, composite PCMs must possess sufficiently high energy storage capacities. In this study, thermal performance parameters, including the melting/freezing temperature (T_m/T_f) and melting/freezing enthalpy ($\Delta H_m/\Delta H_f$) of the 3D-Mt/PEG composite PCMs, were investigated by using DSC. The DSC curves illustrating the melting and freezing behaviors of PEG and the 3D-Mt/PEG composite PCMs are presented in Fig. 4(a) and (b). In terms of phase change enthalpy (Fig. 4(c)), the ΔH_m and ΔH_f of pure PEG were 208.56 and 192.35 J/g, respectively. For comparison, the ΔH_m and ΔH_f of the 3D-Mt/PEG composite PCMs were 167.53 and 161.12 J/g, respectively. Compared with that of pure PEG, the heat storage capacity of the 3D-Mt/PEG composite PCMs had slightly reduced because 3D-Mt lacks phase change ability. The supercooling issue is a prominent limitation in the practical implementation of the 3D-Mt/PEG composite PCMs. It is predominantly attributed to the PCMs' inadequate self-nucleation ability during crystallization. This characteristic ultimately impairs the storage of latent heat. The subcooling value is the difference between T_m and T_f. Fig. 4(d) shows that the T_m and T_f of pure PEG were 60.56 and 44.26°C, respectively. Correspondingly, the T_m and T_f of the 3D-Mt/PEG composite PCMs were 62.11 and 49.03°C, respectively. The calculated supercooling degrees of PEG and 3D-Mt/PEG were 16.3 and 13.08°C, respectively. The undercooling of 3D-Mt/PEG had decreased by 19.75% relative to that of pure PEG, primarily due to the heterogeneous nucleation action of 3D-Mt that promoted the crystallization of PEG [46]. The results show that 3D-Mt/PEG can effectively reduce the undercooling of PEG.

Two important parameters, namely, packing ratio (R) and packing efficiency (E), were used to further characterize the phase transition performance of the composite PCMs. DSC results were calculated by using the following formula [47–49]:

$$R = \frac{H_{m,composite\ PCMs}}{H_{m,PEG}} \times 100\% \qquad (1)$$

$$E = \frac{H_{m,composite\ PCMs} + H_{f,composite\ PCMs}}{H_{m,PEG} + H_{f,PEG}} \times 100\% \qquad (2)$$

where $H_{m,composite\ PCMs}$ and $H_{f,composite\ PCMs}$ denote the melting and freezing enthalpy of the 3D-Mt/PEG composite PCMs, respectively, whereas $H_{m,PEG}$ and $H_{f,PEG}$ represent the
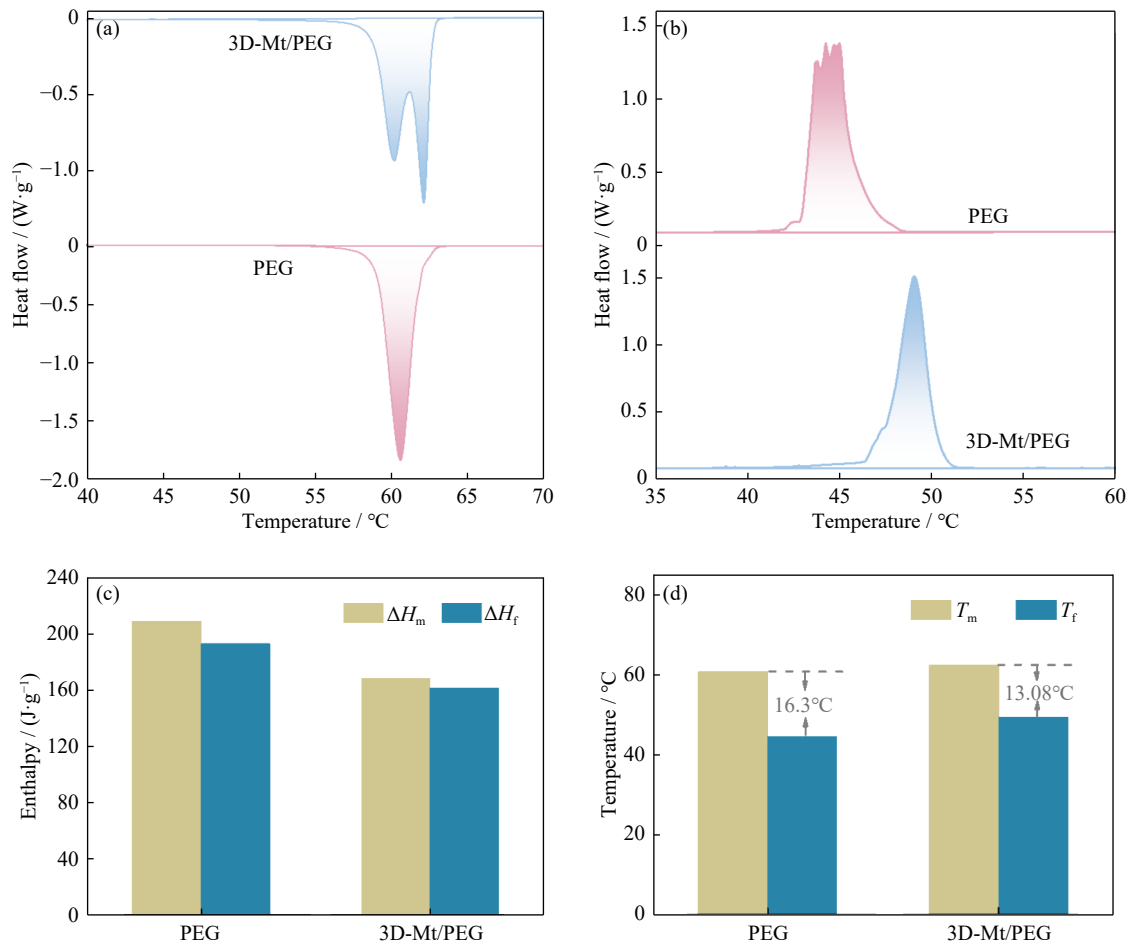
Fig. 4.   DSC curves of (a) melting and (b) cooling, (c) phase transition enthalpy, and (d) peak phase transition temperature of pure PEG and 3D-Mt/PEG composite PCMs.

melting and freezing enthalpy of PEG, respectively. The calculated R and E of the 3D-Mt/PEG composite PCMs were 80.33% and 81.98%, respectively. These results demonstrate that the composite PCMs can effectively encapsulate a large amount of PEG in their 3D pore structure as well as effectively store and release heat through phase transformation.

Table 1 shows that compared with the mineral-based composite PCMs with layered/porous, core–shell, and network packaging reported in the literature, the 3D-Mt materials with a vertical porous structure designed in this work exhibits excellent packing efficiency, highlighting its promising potential for applications in thermal energy storage.

Table 1.   Comparison of the latent heats of the 3D-Mt/PEG composites with those of previously prepared mineral-based composite PCMs

| Packaging method | Samples | Melting process | | Freezing process | | Weight fraction of PCMs / % | Refs. |
		T_m / °C	ΔH_m / (J·g^{-1})	T_f / °C	ΔH_f / (J·g^{-1})		
Layered/porous packaging	Stearic acid/kaolin	53.86	66.3	52.91	65.6	39.0	[50]
	PEG/fly ash	56.55	88.38	36.97	79.87	48.45	[51]
	Stearic acid/isocyanate-functionalized palygorskite	69.71	153.1	66.55	139.9	75.63	[52]
	Capric–myristic–stearic acid eutectic mixture/modified expanded vermiculite	22.92	86.4	21.03	80.4	53.29	[53]
Core–shell packaging	Ag–paraffin@halloysite	57.93	150.58	61.82	136.42	83.89	[54]
	Al–Si@Al$_2$O$_3$@mullite	575	367.1	510	298.4	78.8	[55]
	Mt/stearic acid	63.20	161.87	69.36	166.21	78.70	[56]
	Capric acid@colemanite-doped melamine formaldehyde	31.74	89.83	22.35	91.91	54	[57]
Network packaging	Palygorskite/pectin aerogels–dodecylamine	37.38	210.6	18.66	224.7	80.61	[58]
	Hectorite aerogel–octadecane	27.49	196.70	25.87	197.19	85.96	[59]
	3D-Mt/PEG	62.11	167.53	49.03	161.12	81.98	This work

3.4. Heat transfer performance

Thermal response and heat conduction remarkably affect the heat storage efficiency of PCMs. An IR camera was employed to capture IR images at various intervals to observe visually the transient temperature response and heat conduction of the 3D-Mt/PEG composite PCMs during heating. In this experiment, the composite PCMs and pure PEG were placed under a xenon lamp, which acted as a heat source through illumination. Fig. 5(a) displays the top view of the IR thermal image. The image shows that the 3D-Mt/PEG composite PCMs had a highly sensitive thermal response, leading to a rapid rise in temperature. After 60 s of illumination, the temperature of the composite PCMs rose to 52.7°C from room temperature, whereas that of pure PEG only increased to 33.6°C. The side-view IR thermal image (Fig. 5(b)) demonstrates that the 3D-Mt/PEG composite PCMs exhibited a faster heating rate than pure PEG. This enhancement is primarily attributed to the vertical sheet structure of 3D-Mt, which establishes vertical heat transfer channels in the composite PCMs. Therefore, under illuminated conditions, heat can be quickly and directionally transferred so that the tem-

perature of the upper and lower surface of the samples tend to become consistent in a short time. The excellent radial thermal conductivity and thermal diffusion rate of 3D-Mt shown in Fig. 5(c) also support this result. The results indicate that the interconnected 3D structure of 3D-Mt can serve as a complete heat conduction network, achieving rapid and uniform heat distribution, which is beneficial for heat storage by PEG in composite PCMs.

3.5. Shape stability and thermal stability

The thermal stability of the 3D-Mt/PEG composite PCMs was investigated by using TG under a nitrogen atmosphere (Fig. 6(a)). Pure PEG exhibits a typical one-step thermal degradation process, starting to decompose at 200°C and completely degrading at 420°C mainly through molecular chain scission and pyrolysis [60–61]. The weight loss of 3D-Mt involves three stages, each attributed to specific factors: the evaporation of water within samples, decomposition of functional groups along the sodium alginate polymer chain within samples, and degradation of the main sodium alginate chain [62–63]. In the TG curve of the 3D-Mt/PEG composite PCMs, the slight weight loss at temperature below 200°C
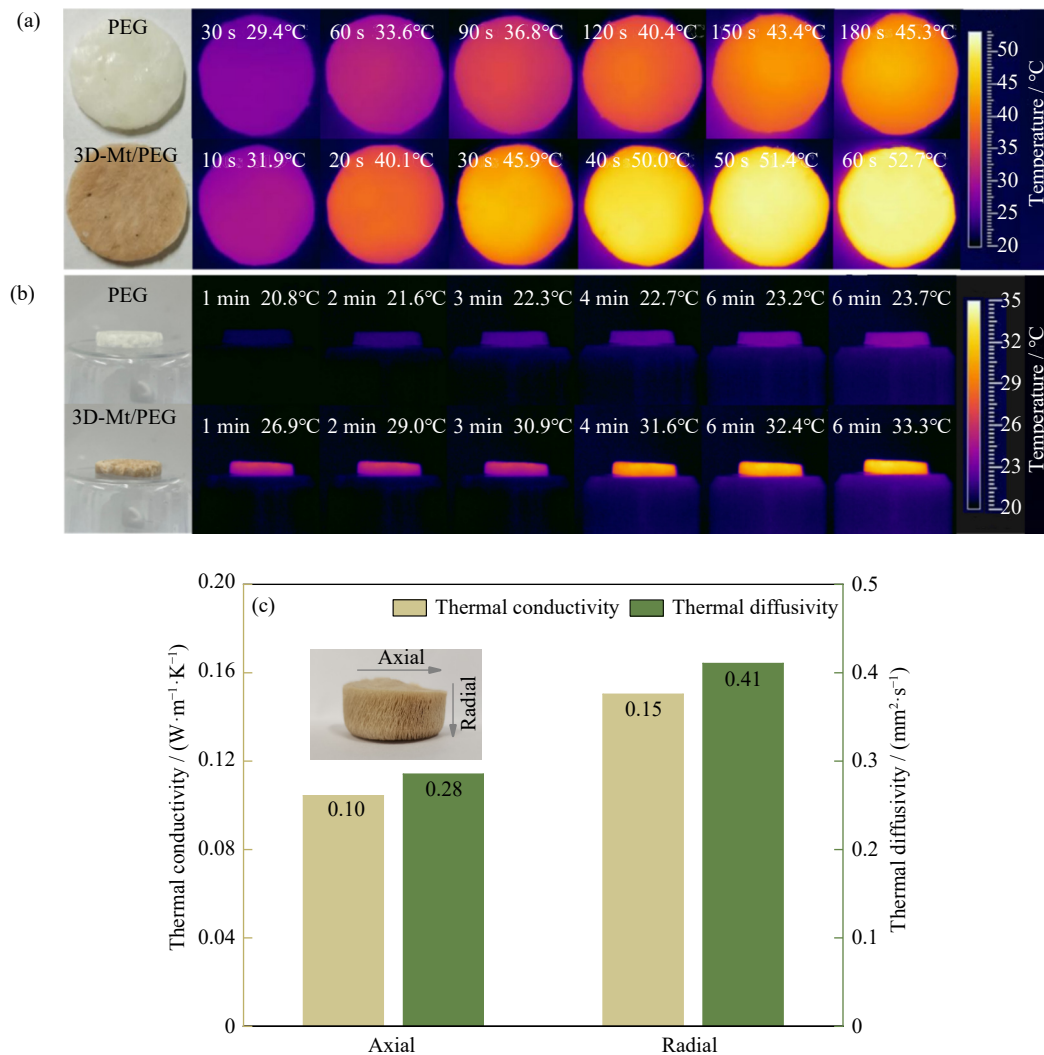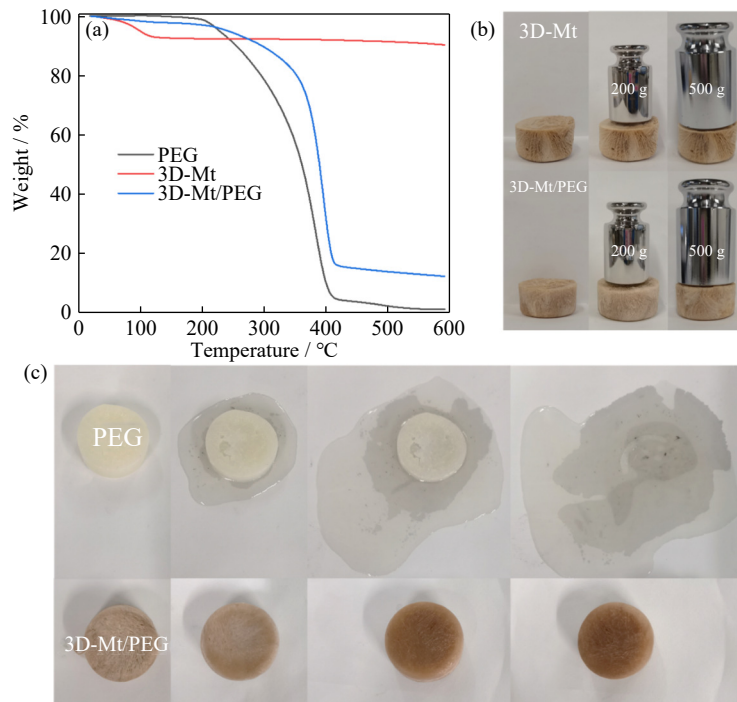

Fig. 5.   (a) Top-view and (b) side-view IR thermal images of pure PEG and the 3D-Mt/PEG composite PCMs under solar irradiation, (c) anisotropy of thermal conductivity and thermal diffusivity of 3D-Mt.

Fig. 6. **(a) TG curves and (b) mechanical strength of PEG, 3D-Mt, and the 3D-Mt/PEG composite PCMs, (c) shape stability of PEG and the 3D-Mt/PEG composite PCMs during heating.**

was due to the evaporation of the adsorbent water of the sample, whereas the mass loss at temperature above 200°C was mainly caused by the degradation of PEG and 3D-Mt. These results demonstrate that the 3D-Mt/PEG composite PCMs exhibit favorable thermal stability at temperature below 200°C.

The practical utilization of 3D-Mt/PEG PCMs critically hinges on their shape stability, including the structure not being destroyed by external forces and the PEG in the pores not leaking after melting. For this reason, the mechanical strength and leak resistance of the composite PCMs were tested. As depicted in Fig. 6(b), the 3D-Mt/PEG composite PCMs exhibit outstanding mechanical strength and can endure a weight of 500 g without deformation. For further exploration of the materials' shape stability, the 3D-Mt/PEG composite PCMs and pure PEG were positioned on a heating plate to observe any potential leakage during heating. As shown in Fig. 6(c), the pure PEG melted into a flowable liquid and spread on the paper, whereas the 3D-Mt/PEG composite PCMs maintained their shape integrity and did not show remarkable leakage. The exceptional shape stability of the composite PCMs primarily results from the robust support provided by the porous 3D-Mt structure to the molten PEG. This support is complemented by the effective capillary force that secured the molten PEG in place.

3.6. Cycling stability

The samples were subjected to 50 melting/freezing cycles to investigate the cycling stability of the 3D-Mt/PEG composite PCMs. As depicted in Fig. 7, no substantial changes in phase transition temperature and enthalpy were observed. The melting and freezing temperature peaks changed from 62.50 and 50.28°C to 62.09 and 50.42°C, respectively. Melt-

ing and freezing enthalpies negligibly decreased from 157.0 and 150.1 J/g to 155.2 and 148.0 J/g, respectively. The cycling test shows that the 3D-Mt/PEG composite PCMs have excellent reusability.

3.7. Flame resistance of the composite PCMs

Microcombustion calorimetry (MCC) was employed to investigate the chemical calorific values of pure PEG and the 3D-Mt/PEG composite PCMs. Peak heat release rate (PHRR), temperature at PHHR (TPHRR), and total heat release rate (THR) were the key parameters used to evaluate the flame retardancy of the 3D-Mt/PEG composite PCMs. Fig. 8 illustrates the heat release rate (HRR) curves of pure PEG and the 3D-Mt/PEG composites, and the corresponding parameters are summarized in Table 2.

The results showed that pure PEG was highly flammable, with the PHRR and THR of 432.7 W/g and 21.8 kJ/g, respectively. The PHRR and THR of the composite PCMs obtained after PEG encapsulation in 3D-Mt were 248.5 W/g and 20.3 kJ/g, respectively. Compared with pure PEG, the 3D-Mt/PEG composite PCMs exhibited a decrease in THR by 6.88% and a notable reduction in PHRR by 42.57%. These findings indicate that the 3D-Mt network can effectively retard flame propagation, serving as a barrier and enhancing the fire safety of the composite PCMs.

4. Conclusion

This work introduces novel composite PCMs based on Mt aerogel. 3D-Mt was synthesized via freeze-drying, and PEG was incorporated into the aerogel framework through vacuum impregnation, resulting in the formation of the 3D-Mt/PEG composite PCMs, which are characterized by stable
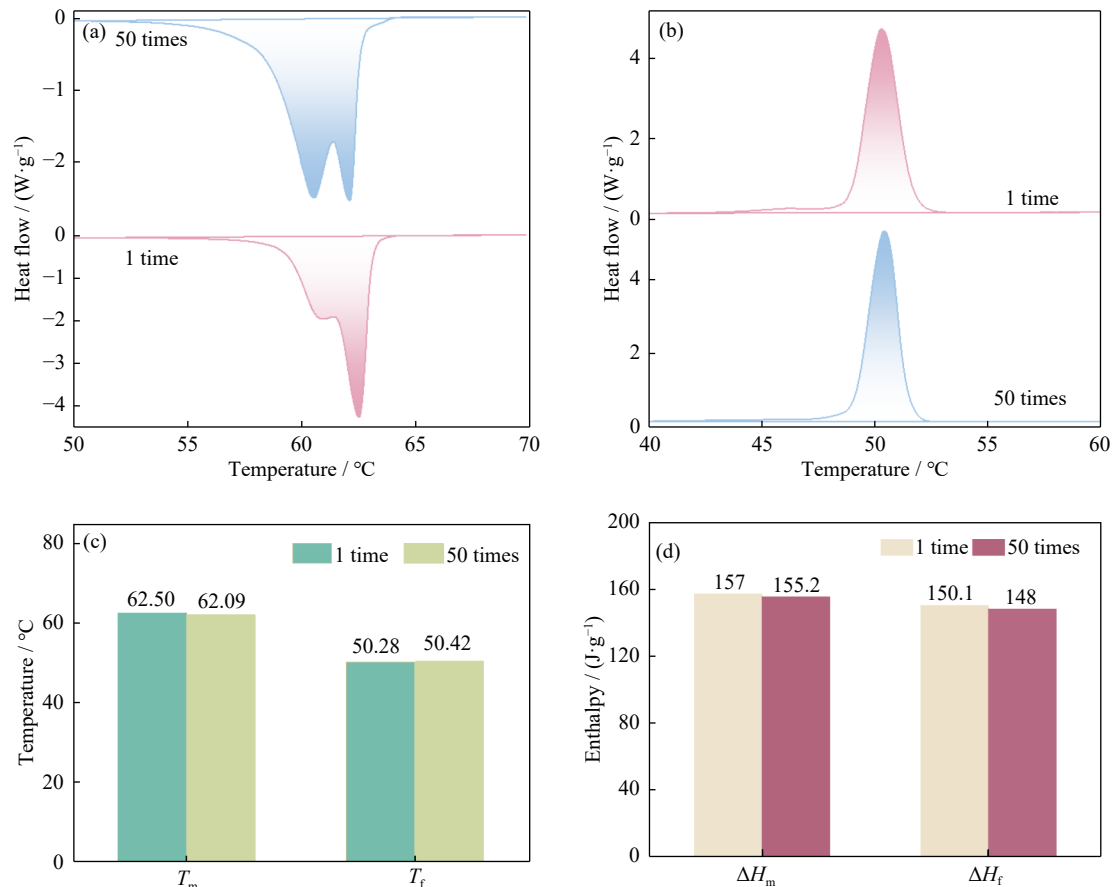
Fig. 7. (a) Melting and (b) cooling DSC diagrams, (c) peak phase transition temperature, and (d) phase transition enthalpy of 3D-Mt/PEG in heating and cooling cycle performance tests.
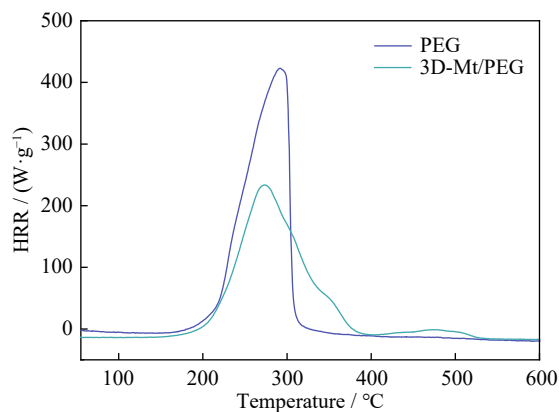

Fig. 8. HRR curves of pure PEG and the 3D-Mt/PEG composite PCMs.

Table 2. Microcombustion calorimetry parameters of pure PEG and the 3D-Mt/PEG composite PCMs

Sample	PHRR / (W·g^{-1})	TPHRR / °C	THR / (kJ·g^{-1})
PEG	432.7	291.4	21.8
3D-Mt/PEG	248.5	272.8	20.3

performance and commendable flame retardancy. The composite PCMs not only exhibit high thermal energy storage density and good cycle stability but also maintain excellent shape stability. Compared with that of pure PEG, the PHRR of the 3D-Mt/PEG composite PCMs has decreased by 42.57%, indicating increased fire safety. The considerably

enhanced temperature response and directional thermal conductivity of the composite PCMs increase energy storage efficiency. Therefore, the PCMs developed in this work have considerable potential for various thermal energy applications. This research offers a novel approach for designing and preparing high-performance composite PCMs, signifying considerable potential in mitigating the energy crisis.

Acknowledgement

Conflict of Interest

Shaoxian Song is an editorial board member for this journal and was not involved in the editorial review or the decision to publish this article. The authors declare that they have no known competing financial interests or personal relationships that could have appeared to influence the work reported in this paper.

References

[1] K. Pielichowska and K. Pielichowski, Phase change materials for thermal energy storage, *Prog. Mater. Sci.*, 65(2014), p. 67.
[2] L.S. Tang, J. Yang, R.Y. Bao, *et al.*, Polyethylene

glycol/graphene oxide aerogel shape-stabilized phase change materials for photo-to-thermal energy conversion and storage via tuning the oxidation degree of graphene oxide, *Energy Convers. Manage.*, 146(2017), p. 253.

[3] Z.D. Tang, H.Y. Gao, X. Chen, Y.F. Zhang, A. Li, and G. Wang, Advanced multifunctional composite phase change materials based on photo-responsive materials, *Nano Energy*, 80(2021), art. No. 105454.

[4] H.Y. Wu, S.T. Li, Y.W. Shao, *et al.*, Melamine foam/reduced graphene oxide supported form-stable phase change materials with simultaneous shape memory property and light-to-thermal energy storage capability, *Chem. Eng. J.*, 379(2020), art. No. 122373.

[5] Q.J. Guo, H. Yi, F.F. Jia, and S.X. Song, Design of MoS₂/MMT bi-layered aerogels integrated with phase change materials for sustained and efficient solar desalination, *Desalination*, 541(2022), art. No. 116028.

[6] B.Y. Gong, H.C. Yang, S.H. Wu, *et al.*, Phase change material enhanced sustained and energy-efficient solar-thermal water desalination, *Appl. Energy*, 301(2021), art. No. 117463.

[7] S. Aghakhani, A. Ghaffarkhah, M. Arjmand, N. Karimi, and M. Afrand, Phase change materials: Agents towards energy performance improvement in inclined, vertical, and horizontal walls of residential buildings, *J. Build. Eng.*, 56(2022), art. No. 104656.

[8] S.R.L. da Cunha and J.L.B. de Aguiar, Phase change materials and energy efficiency of buildings: A review of knowledge, *J. Energy Storage*, 27(2020), art. No. 101083.

[9] Q.R. Zhang, T.T. Xue, J. Tian, Y. Yang, W. Fan, and T.X. Liu, Polyimide/boron nitride composite aerogel fiber-based phase-changeable textile for intelligent personal thermoregulation, *Compos. Sci. Technol.*, 226(2022), art. No. 109541.

[10] K.Y. Sun, H.S. Dong, Y. Kou, *et al.*, Flexible graphene aerogel-based phase change film for solar-thermal energy conversion and storage in personal thermal management applications, *Chem. Eng. J.*, 419(2021), art. No. 129637.

[11] Y. Lu, X.D. Xiao, J. Fu, *et al.*, Novel smart textile with phase change materials encapsulated core-sheath structure fabricated by coaxial electrospinning, *Chem. Eng. J.*, 355(2019), p. 532.

[12] X.C. Wang, G.Y. Li, G. Hong, Q. Guo, and X.T. Zhang, Graphene aerogel templated fabrication of phase change microspheres as thermal buffers in microelectronic devices, *ACS Appl. Mater. Interfaces*, 9(2017), No. 47, p. 41323.

[13] J. Luo, D.Q. Zou, Y.S. Wang, S. Wang, and L. Huang, Battery thermal management systems (BTMs) based on phase change material (PCM): A comprehensive review, *Chem. Eng. J.*, 430(2022), art. No. 132741.

[14] J. Shon, H. Kim, and K. Lee, Improved heat storage rate for an automobile coolant waste heat recovery system using phase-change material in a fin–tube heat exchanger, *Appl. Energy*, 113(2014), p. 680.

[15] S. Gong, X.L. Li, M.J. Sheng, *et al.*, High thermal conductivity and mechanical strength phase change composite with double supporting skeletons for industrial waste heat recovery, *ACS Appl. Mater. Interfaces*, 13(2021), No. 39, p. 47174.

[16] H. Nazir, M. Batool, F.J.B. Osorio, *et al.*, Recent developments in phase change materials for energy storage applications: A review, *Int. J. Heat Mass Transf.*, 129(2019), p. 491.

[17] D.C. Gao, Y.J. Sun, A.M. Fong, and X.B. Gu, Mineral-based form-stable phase change materials for thermal energy storage: A state-of-the art review, *Energy Storage Mater.*, 46(2022), p. 100.

[18] D.Y. Zhang, C.C. Li, N.Z. Lin, B.S. Xie, and J. Chen, Mica-stabilized polyethylene glycol composite phase change materials for thermal energy storage, *Int. J. Miner. Metall. Mater.*, 29(2022), No. 1, p. 168.

[19] C.C. Li, X.K. Peng, J.J. He, and J. Chen, Modified sepiolite sta-

[20] T.T. Qian, J.H. Li, X. Min, Y. Deng, W.M. Guan, and L. Ning, Diatomite: A promising natural candidate as carrier material for low, middle and high temperature phase change material, *Energy Convers. Manage.*, 98(2015), p. 34.

[21] M. Li and Z.S. Wu, A review of intercalation composite phase change material: Preparation, structure and properties, *Renewable Sustainable Energy Rev.*, 16(2012), No. 4, p. 2094.

[22] P.Z. Lv, C.Z. Liu, and Z.H. Rao, Review on clay mineral-based form-stable phase change materials: Preparation, characterization and applications, *Renewable Sustainable Energy Rev.*, 68(2017), p. 707.

[23] M. Li, Z.S. Wu, H.T. Kao, and J.M. Tan, Experimental investigation of preparation and thermal performances of paraffin/bentonite composite phase change material, *Energy Convers. Manage.*, 52(2011), No. 11, p. 3275.

[24] J. Giro-Paloma, M. Martínez, L.F. Cabeza, and A. Inés Fernández, Types, methods, techniques, and applications for microencapsulated phase change materials (MPCM): A review, *Renewable Sustainable Energy Rev.*, 53(2016), p. 1059.

[25] G. Alva, Y.X. Lin, L.K. Liu, and G.Y. Fang, Synthesis, characterization and applications of microencapsulated phase change materials in thermal energy storage: A review, *Energy Build.*, 144(2017), p. 276.

[26] H. Yi, W.Q. Zhan, Y.L. Zhao, *et al.*, A novel core–shell structural montmorillonite nanosheets/stearic acid composite PCM for great promotion of thermal energy storage properties, *Sol. Energy Mater. Sol. Cells*, 192(2019), p. 57.

[27] Z. Sun, L.J. Zhao, H.X. Wan, H. Liu, D.Z. Wu, and X.D. Wang, Construction of polyaniline/carbon nanotubes-functionalized phase-change microcapsules for thermal management application of supercapacitors, *Chem. Eng. J.*, 396(2020), art. No. 125317.

[28] Z. Zhang, Z. Zhang, T. Chang, J. Wang, X. Wang, and G.F. Zhou, Phase change material microcapsules with melamine resin shell via cellulose nanocrystal stabilized Pickering emulsion *in situ* polymerization, *Chem. Eng. J.*, 428(2022), art. No. 131164.

[29] P. Liu, X. Chen, Y. Li, *et al.*, Aerogels meet phase change materials: Fundamentals, advances, and beyond, *ACS Nano*, 16(2022), No. 10, p. 15586.

[30] S. Kashyap, S. Kabra, and B. Kandasubramanian, Graphene aerogel-based phase changing composites for thermal energy storage systems, *J. Mater. Sci.*, 55(2020), No. 10, p. 4127.

[31] H. Yi, Z. Ai, Y.L. Zhao, X. Zhang, and S.X. Song, Design of 3D-network montmorillonite nanosheet/stearic acid shape-stabilized phase change materials for solar energy storage, *Sol. Energy Mater. Sol. Cells*, 204(2020), art. No. 110233.

[32] H.Z. Hong, Y. Pan, H.X. Sun, *et al.*, Superwetting polypropylene aerogel supported form-stable phase change materials with extremely high organics loading and enhanced thermal conductivity, *Sol. Energy Mater. Sol. Cells*, 174(2018), p. 307.

[33] M. Cheng, J. Hu, J.Q. Xia, *et al.*, One-step *in situ* green synthesis of cellulose nanocrystal aerogel based shape stable phase change material, *Chem. Eng. J.*, 431(2022), art. No. 133935.

[34] Q.J. Guo, Q. An, H. Yi, F.F. Jia, and S.X. Song, Double-layered montmorillonite/MoS₂ aerogel with vertical channel for efficient and stable solar interfacial desalination, *Appl. Clay Sci.*, 217(2022), art. No. 106389.

[35] D.Y. Liu, C.X. Lei, K. Wu, and Q. Fu, A multidirectionally thermoconductive phase change material enables high and durable electricity *via* real-environment solar-thermal-electric conversion, *ACS Nano*, 14(2020), No. 11, p. 15738.

[36] R.I. Iliescu, E. Andronescu, C.D. Ghitulica, G. Voicu, A. Ficai, and M. Hoteteu, Montmorillonite-alginate nanocomposite as a

drug delivery system: Incorporation and *in vitro* release of irinotecan, *Int. J. Pharm.*, 463(2014), No. 2, p. 184.

[37] A. Olad, M. Pourkhiyabi, H. Gharekhani, and F. Doustdar, Semi-IPN superabsorbent nanocomposite based on sodium alginate and montmorillonite: Reaction parameters and swelling characteristics, *Carbohydr. Polym.*, 190(2018), p. 295.

[38] H. Yi, L. Xia, and S.X. Song, Three-dimensional montmorillonite/Ag nanowire aerogel supported stearic acid as composite phase change materials for superior solar-thermal energy harvesting and storage, *Compos. Sci. Technol.*, 217(2022), art. No. 109121.

[39] Q.J. Guo, H. Yi, F.F. Jia, and S.X. Song, Vertical porous MoS_2/hectorite double-layered aerogel as superior salt resistant and highly efficient solar steam generators, *Renewable Energy*, 194(2022), p. 68.

[40] E.R. Kenawy, M.M. Azaam, and E.M. El-nshar, Sodium alginate-g-poly(acrylic acid-co-2-hydroxyethyl methacrylate)/montmorillonite superabsorbent composite: Preparation, swelling investigation and its application as a slow-release fertilizer, *Arab. J. Chem.*, 12(2019), No. 6, p. 847.

[41] E. Tao, D. Ma, S.Y. Yang, and X. Hao, Graphene oxide-montmorillonite/sodium alginate aerogel beads for selective adsorption of methylene blue in wastewater, *J. Alloys Compd.*, 832(2020), art. No. 154833.

[42] W. Wang, C.Y. Zhang, J.Y. He, *et al.*, Chitosan-induced self-assembly of montmorillonite nanosheets along the end-face for methylene blue removal from water, *Int. J. Biol. Macromol.*, 227(2023), p. 952.

[43] W. Wang, T. Wen, and H.Y. Bai, , Adsorption toward Cu(II) and inhibitory effect on bacterial growth occurring on molybdenum disulfide-montmorillonite hydrogel surface, *Chemosphere*, 248(2020), art. No. 126025.

[44] Y. Zhou, X.D. Liu, D.K. Sheng, *et al.*, Polyurethane-based solid-solid phase change materials with *in situ* reduced graphene oxide for light-thermal energy conversion and storage, *Chem. Eng. J.*, 338(2018), p. 117.

[45] Y. Zhou, D.K. Sheng, X.D. Liu, *et al.*, Synthesis and properties of crosslinking halloysite nanotubes/polyurethane-based solid–solid phase change materials, *Sol. Energy Mater. Sol. Cells*, 174(2018), p. 84.

[46] H.H. Liao, W.H. Chen, Y. Liu, and Q. Wang, A phase change material encapsulated in a mechanically strong graphene aerogel with high thermal conductivity and excellent shape stability, *Compos. Sci. Technol.*, 189(2020), art. No. 108010.

[47] T.T. Qian, J.H. Li, X. Min, W.M. Guan, Y. Deng, and L. Ning, Enhanced thermal conductivity of PEG/diatomite shape-stabilized phase change materials with Ag nanoparticles for thermal energy storage, *J. Mater. Chem. A*, 3(2015), No. 16, p. 8526.

[48] X. Chen, H.Y. Gao, M. Yang, *et al.*, Highly graphitized 3D network carbon for shape-stabilized composite PCMs with superior thermal energy harvesting, *Nano Energy*, 49(2018), p. 86.

[49] S.Y. Yu, X.D. Wang, and D.Z. Wu, Microencapsulation of n-octadecane phase change material with calcium carbonate shell for enhancement of thermal conductivity and serving durability:

Synthesis, microstructure, and performance evaluation, *Appl. Energy*, 114(2014), p. 632.

[50] S.Y. Liu and H.M. Yang, Stearic acid hybridizing coal–series Kaolin composite phase change material for thermal energy storage, *Appl. Clay Sci.*, 101(2014), p. 277.

[51] J.M.Gao, S.J. Ma, B. Wang, Z.B. Ma, Y.X. Guo, and F.Q. Cheng, Template-free facile preparation of mesoporous silica from fly ash for shaped composite phase change materials, *J. Cleaner Prod.*, 384 (2023), art. No. 135583.

[52] Y. Wang, Y.H. Song, S. Li, T. Zhang, D.Y. Zhang, and P.R. Guo, Thermophysical properties of three-dimensional palygorskite based composite phase change materials, *Appl. Clay Sci.*, 184(2020), art. No. 105367.

[53] H.T. Wei, X.Z. Xie, X.Q. Li, and X.S. Lin, Preparation and characterization of capric–myristic–stearic acid eutectic mixture/modified expanded vermiculite composite as a form-stable phase change material, *Appl. Energy*, 178(2016), p. 616.

[54] Y.F. Zhao, W.X. Kong, Z.L. Jin, *et al.*, Storing solar energy within Ag–paraffin@Halloysite microspheres as a novel self-heating catalyst, *Appl. Energy*, 222(2018), p. 180.

[55] C.J. Han, H.Z. Gu, M.J. Zhang, A. Huang, Y. Zhang, and Y. Wang, Al–Si@Al_2O_3@mullite microcapsules for thermal energy storage: Preparation and thermal properties, *Sol. Energy Mater. Sol. Cells*, 217(2020), art. No. 110697.

[56] H. Yi, W.Q. Zhan, Y.L. Zhao, *et al.*, Design of MtNS/SA microencapsulated phase change materials for enhancement of thermal energy storage performances: Effect of shell thickness, *Sol. Energy Mater. Sol. Cells*, 200(2019), art. No. 109935.

[57] A.M. Turan and Y. Konuklu, Developing of capric acid@colemanite doped melamine formaldehyde microcapsules and composites as novel thermal energy storage materials, *Therm. Sci. Eng. Prog.*, 41(2023), art. No. 101806.

[58] L.Q. Wang, W.D. Liang, Y. Liu, *et al.*, Carbonized clay pectin-based aerogel for light-to-heat conversion and energy storage, *Appl. Clay Sci.*, 224 (2022), art. No. 106524.

[59] J.H. Zhu, Q. An, Q.J. Guo, H. Yi, L. Xia, and S.X. Song, Mechanically strong hectorite aerogel encapsulated octadecane as shape-stabilized phase change materials for thermal energy storage and management, *Appl. Clay Sci.*, 223(2022), art. No. 106511.

[60] J.R. Li, L.H. He, T.Z. Liu, X.J. Cao, and H.Z. Zhu, Preparation and characterization of PEG/SiO_2 composites as shape-stabilized phase change materials for thermal energy storage, *Sol. Energy Mater. Sol. Cells*, 118(2013), p. 48.

[61] B.M. Li, D. Shu, R.F. Wang, *et al.*, Polyethylene glycol/silica (PEG@SiO_2) composite inspired by the synthesis of mesoporous materials as shape-stabilized phase change material for energy storage, *Renewable Energy*, 145(2020), p. 84.

[62] R.M. Nair, B. Bindhu, and V.L. Reena, A polymer blend from Gum Arabic and sodium alginate-preparation and characterization, *J. Polym. Res.*, 27(2020), No. 6, art. No. 154.

[63] T.M.M. Swamy, B. Ramaraj, and Siddaramaiah, Sodium alginate and poly(ethylene glycol) blends: Thermal and morphological behaviors, *J. Macromol. Sci. Part A*, 47(2010), No. 9, p. 877.